



Bone marrow mesenchymal stem cells loaded into hydrogel/nanofiber composite scaffolds ameliorate ischemic brain injury



Yanhong Pei ^{a, b}, Lifei Huang ^c, Tong Wang ^c, Qinhan Yao ^a, Yanrong Sun ^a, Yan Zhang ^a, Xiaomei Yang ^a, Jiliang Zhai ^d, Lihua Qin ^a, Jiajia Xue ^{c, **}, Xing Wang ^{c, ***}, Hongquan Zhang ^{a, b, ****}, Junhao Yan ^{a, e, *}

^a Department of Human Anatomy, Histology and Embryology, School of Basic Medical Sciences, Peking University Health Science Center, Beijing, 100191, China

^b Program for Cancer and Cell Biology, Department of Human Anatomy, Histology and Embryology, PKU International Cancer Institute, MOE Key Laboratory of Carcinogenesis and Translational Research and State Key Laboratory of Natural and Biomimetic Drugs, Peking University Health Science Center, Beijing, 100191, China

^c State Key Laboratory of Organic-Inorganic Composites, Beijing Laboratory of Biomedical Materials, Beijing University of Chemical Technology, Beijing, 100029, China

^d Department of Orthopedic Surgery, Peking Union Medical College Hospital, Chinese Academy of Medical Science and Peking Union Medical College, Beijing, China

^e Beijing Key Lab of Magnetic Resonance Imaging Technology, Peking University Third Hospital, Beijing, 100191, China

ARTICLE INFO

Article history:

Received 15 November 2022

Received in revised form

10 January 2023

Accepted 21 January 2023

Available online xxx

Keywords:

Bone marrow mesenchymal stem cells

Exosome

Hydrogel

Nanofiber

Ischemic stroke

ABSTRACT

Central nervous system (CNS) function recovery following stroke remains a major challenge because neural regeneration is difficult to achieve. In this study, rigid-flexible composite scaffolds consisting of nanofibers from electrospun scaffolds and self-adapting and injectable hydrogel were loaded with bone marrow mesenchymal stem cells (BMSCs), and the effects of these loaded BMSCs on ischemic insult were investigated. *In vitro* analysis of the viability, migration, neurite growth, angiogenic capacity, and paracrine effects of BMSCs indicated that BMSCs loaded in composite scaffolds had a better therapeutic effect than those BMSCs in saline. Furthermore, *in vivo*, BMSCs loaded in composite scaffolds significantly reduced the extent of brain edema and the infarct volume, alleviated neurological deficits, markedly attenuated microglial and astrocyte overactivation, and increased neuronal proliferation and vascular growth. Bioinformatics analysis revealed that BMSCs loaded in composite scaffolds could decrease the level of exosomal miR-206-3p and consequently increase the activity of the PI3K/AKT signaling pathway. In conclusion, BMSCs loaded in novel composite scaffolds exert obvious neuroprotective effects, attenuating ischemic injury by enhancing angiogenesis and neural regeneration in the brain after ischemic stroke, and these results provide a promising approach for treating CNS diseases in the clinic via cell transplantation.

© 2023 The Authors. Published by Elsevier Ltd. This is an open access article under the CC BY-NC-ND license (<http://creativecommons.org/licenses/by-nc-nd/4.0/>).

* Corresponding author. Department of Anatomy, Histology and Embryology, School of Basic Medical Science, Peking University Health Science Center, No.38 Xueyuan Road, Haidian District, Beijing 100191, China.

** Corresponding author.

*** Corresponding authors.

**** Corresponding author. Program for Cancer and Cell Biology, Department of Human Anatomy, Histology and Embryology, PKU International Cancer Institute, MOE Key Laboratory of Carcinogenesis and Translational Research and State Key Laboratory of Natural and Biomimetic Drugs, Peking University Health Science Center, Beijing, China.

E-mail addresses: jiajiaxue@mail.buct.edu.cn (J. Xue), wangxing@mail.buct.edu.cn (X. Wang), hongquan.zhang@bjmu.edu.cn (H. Zhang), yjh@bjmu.edu.cn (J. Yan).

1. Introduction

Stroke is the main cause of death and disability worldwide, and ischemic stroke is the most common type of stroke [1]. Currently, ischemic stroke treatments aimed at relieving symptoms cannot achieve neural regeneration and neurological function recovery; therefore, novel therapeutic strategies are urgently needed. Stem cell-based therapies are promising approaches for repairing infarcted tissues and improving functional recovery via either trophic support or direct replacement of damaged neurocytes [2,3]. However, the efficacy of stem cell therapies for ischemic stroke is

largely limited due to insufficient cell migration into the infarct zone, the high mortality of transplanted cells, and the poor integration of transplanted cells into the injured brain tissue [4,5].

Tissue engineering scaffolds are designed to mimic the natural extracellular matrix (ECM). Hydrogels and nanofibers are the materials that are most similar to endogenous ECM in the brain. However, due to the inability of hydrogels and nanofibers to dynamically adapt to local defects, their compatibility with nervous tissue is relatively poor. Owing to the dynamic Schiff base network (imine, $-N=CH-$), glycol chitosan (GC) and dibenzaldehyde-terminated polyethylene glycol (DF-PEG) are promising candidates for tissue scaffolds. We mixed short fibers cut from electrospun scaffolds with hydrogel to generate nanofibers 10–300 nm in diameter, similar to those found in the extracellular matrix. The composite material retained the void-filling and shear-thinning characteristics of the hydrogel, which were previously shown to be effective for cell retention, delivery, and minimally invasive biomaterial infusion [6].

Mesenchymal stem cells (MSCs), due to their excellent proliferative ability, competence to be conveniently harvested, multilineage differentiation potential, and immunomodulatory effects, are considered as important cell sources for transplantation after brain injury [7,8]. BMSCs (bone mesenchymal stem cells) are the most well-studied and widely used MSCs for cell transplantation [9]. Exosome release is thought to be the major mechanism underlying the action of BMSCs. Exosomes are extracellular membrane-bound vesicles that range in diameter from 30 to 150 nm, and they are critical to intercellular communication [10]. Exosomes are enriched in small RNAs, especially microRNAs (miRNAs), which are important posttranscriptional regulators that play key roles in CNS damage and repair. It is well known that miRNAs can downregulate the expression of proteins encoded by target mRNAs by binding to the 3'UTR (untranslated region, UTR) [11].

miR-206 is a myomiRNA and plays a significant role in the development of some brain diseases [12]. For example, miR-206 is obviously upregulated and associated with cognitive decline in Alzheimer's disease (AD) patients and mouse models [13]. Additionally, overexpression of miR-206 in the medial prefrontal cortex contributes to a dramatic decrease in the expression level of brain-derived neurotrophic factor (BDNF) and cognitive impairment [12]. However, whether miR-206 is related to ischemic brain injury and the underlying molecular mechanisms remain unknown.

The phosphatidylinositol 3-kinase/protein kinase B (PI3K/Akt) signaling pathway is implicated in hypoxic-ischemic injury [14]. However, it remains to be clarified whether the effects of BMSCs-derived exosomes on ischemic brain injury are dependent on the activity of miR-206 and the PI3K/AKT signaling pathway.

In this study, the neuroprotective roles of BMSCs loaded in composite scaffolds following ischemic stroke were explored, and the potential mechanism involving miR-206 and its modulatory effect on the PI3K/AKT signaling pathway were evaluated.

2. Materials and methods

2.1. Materials

Poly (ethylene glycol) (PEG, Mw = 4000, 96%) was purchased from Sinopharm Group Co. Ltd. Glycol chitosan (GC, 82 kDa, 85% degree of deacetylation) was purchased from Wako Pure Chemical Industries, Ltd., Japan. Other reagents (AR grade) were obtained from Sinopharm Chemical Reagent Co., Ltd. (Shanghai, China).

2.1.1. Synthesis of DF-PEG

Briefly, 6.5 g PEG was dissolved in toluene and then evaporated to dryness on a rotary evaporator. After that, 3.26 g of 4-carboxybenzaldehyde was added to 1.68 g of DCC (N,N'-dicyclohexylcarbodiimide), which was used as a dehydrating agent, and 0.05 g of DMAP (4-dimethylmethaminopyridine), which was used as a catalyst. Then, 30 ml of tetrahydrofuran was added to dissolve the reactants for 24 h, and the mixture was filtered. After 24 h of vacuum drying, solid white DF-PEG was obtained.

2.1.2. Fabrication of the nanofiber

PCL (polycaprolactone) and GelMA (gelatin methacryloyl) solutions (10%, w/v) were used for coaxial electrospinning. GelMA was used as the core polymer, and PCL was used as the shell polymer. The electrospinning parameters were as follows: voltage: 18–20 kV; temperature: 25 °C; distance between the needle and collector: 18 cm. The fibrous membranes were then cut into short fibers (100 μm in length) using a freezing microtome (CM1950, Leica, Germany).

2.1.3. Analysis of rheological and self-adapting properties and mechanical strength

GC solution (3%) was spread onto the parallel plates of a rheometer, and then a uniform droplet of DF-PEG (1%) was placed on the surface. Then, the gelation time was calculated based on the storage modulus G' and the loss modulus G'' . Modulus-frequency tests were conducted using a steel plate (diameter = 20 mm) with 1% strain and 6.3 rad^{-1} . A hydrogel sheet was placed on top of small beads, and whether the hydrogel could pass through the gaps between the beads was tested. A piece of hydrogel (1 ml, 20 mm diameter) was placed on the measuring plate of a rheometer. The storage modulus (G') of the hydrogel was measured at different frequencies (1%, 25 °C).

2.1.4. Preparation of composite scaffolds

Hydrogels were prepared by mixing 1% DF-PEG₄₀₀₀ with 3% GC (1:3). Nanofibers were loaded in the gel at a concentration of 5 mg/ml. The mixed solution was immediately vortexed and pipetted thoroughly.

2.2. BMSCs isolation and culture

Three-to-four-week-old SD rats were euthanized, the tibiae and femurs were extracted, and the bone marrow was flushed out and cultured in α -MEM (32,571,036, Thermo Fisher Scientific, USA) with 10% fetal bovine serum (FBS, 10,091,148, Thermo Fisher Scientific, USA), 100 μg/ml penicillin and 100 μg/ml streptomycin (FB9531, FeiMoBio, China) in a humidified incubator containing 5% CO₂ at 37 °C.

2.3. Cell culture and lentiviral transduction

SH-SY5Y cells were purchased from Procell Co. (Wuhan, China) and were cultured with serum-containing medium (CM-0208, CM-0675, Procell, China).

Stable expression of red fluorescent protein (RFP) was achieved in BMSCs using recombinant lentiviruses (GeneChem, China). BMSCs were transduced with recombinant lentiviruses expressing luciferase (GeneChem, China).

BMSCs in each group were transfected with miR-206–3p agomir, miR-206–3p agomir-NC, miR-206–3p antagomir, or miR-206–3p antagomir-NC (RiboBio, China) at a concentration of 50 nM

using a riboFECT CP Transfection Kit (C10511-05, RiboBio, China) according to the manufacturer's instructions.

2.4. Analysis of cell viability and paracrine capacity under OGD conditions

In this study, an oxygen and glucose deprivation (OGD) model was also established. Briefly, cells were cultured using glucose-free DMEM in a humidified hypoxia incubator (1% oxygen, Ox-101C-50, TOW-INT TECH, China). Cell viability was assessed using two methods. (1) A Live/Dead Cell Double Staining Kit (KTA1001, Abbkine, China) was used to discriminate dead (red) and live (green) cells. (2) A Cell Counting Kit (CCK)-8 (CCK04, Dojindo, Japan) was used to quantify cell viability.

To evaluate the paracrine capacity of BMSCs under OGD conditions, ELISA kits (R1235c, R2603c, R3001, Elabscience, China) were used to measure the levels of brain-derived neurotrophic factor (BDNF), vascular endothelial growth factor (VEGF), and insulin-like growth factor (IGF-1) in conditioned medium (CM).

2.5. Cell migration assay

The SH-SY5Y cell layer was scratched with a sterilized pipette tip, and after 48 h, images were captured with an inverted phase-contrast microscope (IX71, Olympus, Japan). The average extent of wound closure was quantified by ImageJ software (V1.8.0.112, National Institutes of Health, Bethesda, USA) [15].

2.6. Neurite outgrowth assay

SH-SY5Y cells were immunostained for β III tubulin (ab52623, Abcam, USA) to evaluate the average length of the neurites in each group [16].

2.7. HUVEC tube formation assay

The tube networks of human umbilical vein endothelial cells (HUVECs) were observed under bright field microscopy (IX71, Olympus, Japan), and the area and connectivity of the networks were calculated using ImageJ software (V1.8.0.112, National Institutes of Health, Bethesda, USA).

2.8. Bioluminescence imaging with an *in vivo* imaging system (IVIS)

D-luciferin potassium salt (LUCK-100, Goldbio, USA) was injected intraperitoneally, and images were acquired by using an IVIS Spectrum Imaging System (PerkinElmer, USA). Subsequently, the images were analyzed with IVIS Spectrum software (4.3.1 Service Pack 2, Caliper Life Sciences, USA).

2.9. MCAO model establishment

Adult male Sprague Dawley rats weighing 300–320 g (aged 7–8 weeks) were purchased from the Department of Laboratory Animal Science of Peking University Health Science Center. All rats were fed and used in accordance with the regulations of the Experimental Animal Welfare Ethics Committee of Peking University. All procedures performed in this study were approved by the Biomedical Ethics Committee of Peking University. During all experimental procedures, the number of animals and their suffering were minimized.

A middle cerebral artery occlusion (MCAO) model was established by the thread-embolus method of intraluminal vascular occlusion [17]. All rats were anesthetized with an intraperitoneal injection of 1% pentobarbital sodium (40 mg/kg). A thread with a

length of 18.0 mm–22.0 mm (Jialing Biotechnology, China) was inserted through the external carotid artery into the lumen of the internal carotid artery until it blocked the origin of the right MCA. Reperfusion was performed after 1 h of occlusion. Rats in the sham group underwent the same surgery without MCA occlusion. The rectal temperature was maintained at $37\text{ }^{\circ}\text{C} \pm 0.5\text{ }^{\circ}\text{C}$ throughout MCAO.

2.10. Groups and treatment

Rats were randomly divided into 5 groups ($n = 30$ for each group): the sham group, MCAO + saline group, MCAO + Scaffolds group, MCAO + BMSCs group, and MCAO + BMSCs + Scaffolds group.

At 24 h after MCAO (day 0), cell transplantation was performed. Ten microliters of saline, BMSCs suspended in saline (5×10^5 cells/10 μ l) or BMSCs-loaded composite scaffolds were injected into the perilesional site [18] (0.2 mm posterior to bregma, 3.5 mm lateral to bregma, 2.0 mm deep from the skull surface) using a gas-tight Hamilton syringe with a 26 s-gauge needle (80,330, Hamilton, Switzerland) within 10 min.

2.11. Histological analysis

For immunohistochemistry, coronal brain sections (thickness = 30 μ m) were blocked with 10% goat serum and incubated with primary antibodies against Iba-1 (ab178847, Abcam, USA), Nestin (NB100-1604, Novus, USA), CD31 (ab281583, Abcam, USA), and glial fibrillary acidic protein (GFAP, ab7260, Abcam, USA) diluted 1:200 at 4 $^{\circ}\text{C}$ overnight. The sections were then incubated with secondary antibodies (ab150077, ab150120, Abcam, USA) diluted 1:500 at 37 $^{\circ}\text{C}$ for 1.5 h, counterstained with DAPI (S2110, Solarbio, China) and observed under a fluorescence microscope (DP70, Olympus, Japan). Signals were quantitatively evaluated by using ImageJ software (V1.8.0.112, National Institutes of Health, Bethesda, USA).

Composite scaffolds were injected into the back of each rat (100 μ l; at 1, 7, and 14 days). Skin sections were subjected to hematoxylin and eosin (HE) staining using an HE Staining Kit (G1120, Solarbio, China) according to the manufacturer's instructions.

2.12. 2,3,5-Triphenyltetrazolium chloride (TTC) staining

Coronal slices (six slices from each rat brain) at 1 mm intervals in the rostral to the caudal direction were prepared and immersed in 2% TTC at 37 $^{\circ}\text{C}$ for 20 min. Digital images of the caudal aspect of each slice were analyzed using ImageJ software (V1.8.0.112, National Institutes of Health, Bethesda, USA). The percentage of the infarct volume was evaluated as follows: infarct volume/total slice volume \times 100%.

2.13. Analysis of brain water content (BWC)

The brains of the rats in each group were immediately removed and weighed (wet weight). Then, the brains were dried in an oven at 105 $^{\circ}\text{C}$ for 24 h to obtain the dry weight [19]. Brain water content (%) was calculated as (wet weight – dry weight)/wet weight \times 100%.

2.14. Neurobehavioral function assessment

Neurobehavioral function assessments were conducted at 1, 7, and 14 d after MCAO. The assessments included sensory, motor, and balance tests, and scores ranged from 0 to 18 [20].

The rotarod test was used to assess motor coordination and

impairment. Briefly, rats were placed on the apparatus (Harvard Apparatus, Cambridge, UK), and the rotarod speed was slowly increased from 4 to 40 rpm over 5 min. If a rat fell off the rod, gripped the device, or spun twice in a row without trying to walk on the rod, the test was ended.

The beam walking test (BWT) was used to test coordination and recovery of motor function. The time needed to traverse an elevated (90 cm) narrow wooden beam (2.5 cm × 100 cm) and enter a black plastic box (15 cm × 15 cm × 8 cm) at the opposite end was recorded.

2.15. Exosome isolation and miRNA sequencing

When the confluence of BMSCs was almost 60%–70%, the serum-containing medium was replaced with serum-free medium for 48 h. Then, the cell supernatants were collected and ultra-centrifuged for exosome extraction.

The morphology and size distribution of the exosomes were assessed by transmission electron microscopy (TEM) and dynamic light scattering (DLS) analysis. The exosome-associated surface proteins CD9 (555,371, BD, USA), CD63 (557,288, BD, USA), and CD81 (557,108, BD, USA) were detected by flow cytometry.

miRNAs were isolated from exosomes using a miRNeasy Mini Kit (217,004, Qiagen, Germany). A small RNA sequencing library was prepared using a QIAseq® miRNA Library Kit (331,505, Qiagen, Germany). Sequencing was performed on the Illumina Nova-Seq6000 and PE150 platforms. In brief, double-end sequencing reads were cleaned with a quality filter, adapter cutter, and length filter using the NCBI assembly mRatBN7.2, mirbase-22-release. Differentially expressed miRNAs were identified using a fold-change cutoff of ≥ 2.0 for both up- and down-regulated genes.

2.16. Dual-luciferase reporter assay

Reporter vectors expressing wild-type and mutant binding sites (pGL3-PI3K-1394 Mut) were constructed and transfected with miR-206–3p mimics and pRL-TK (an internal reference plasmid expressing Renilla luciferase) into HEK293T cells (CL-0005, Pricella, China). The ratio of Firefly/Renilla activity was calculated to assess relative luciferase activity by using a Dual-Luciferase® Reporter Assay Kit (E1910, Promega, USA).

2.17. Proteome sequencing and western blotting

Tandem mass tag (TMT)-based proteomics analyses were performed to identify differentially expressed proteins (DEPs). Significantly differentially expressed proteins were screened with the fold change cutoff of ≥ 2.0 and *P* value cutoff of < 0.05 . Kyoto Encyclopedia of Genes and Genomes (KEGG) pathway analysis and Gene Ontology (GO) and Wiki pathway analysis using the WEB-Based Gene Set Analysis Tool Kit were carried out with Fisher's exact test, and FDR correction for multiple testing was also performed.

Brain tissues from the ischemic penumbra area (approximately 30 mg) were lysed using RIPA lysis buffer (C1053, Applygen, China) supplemented with protease and phosphatase inhibitors (P1261, Applygen, China) and centrifuged (12,000×g, 30 min, 4 °C). Membranes were probed with the following primary antibodies in 5% BSA-TBST overnight at 4 °C: p-PI3K (bs-6417 R, Bioss, China), PI3K (A0982, Abclonal, China), p-AKT (4060 T, CST, USA), AKT (4691 T, CST, USA), VEGFR2 (vascular endothelial growth factor receptor 2, VEGFR2), (9698 S, CST, USA), VEGFA (vascular endothelial growth factor A, VEGFA) (ab214424, Abcam, USA), cleaved caspase-3 (9664 S, CST, USA), and GAPDH (glyceraldehyde-3-phosphate dehydrogenase, GAPDH) (5174 T, CST, USA). Then, the membranes

were incubated with HRP-conjugated secondary antibody (7074 S, CST, USA) for 1 h at room temperature. The blots were developed by a chemiluminescence assay (1,705,060, Bio-Rad, USA).

2.18. Quantitative RT-PCR (qRT-PCR)

Total RNA was extracted from cells using RNA-Easy Isolation Reagent (DP424, Tiangen, China) and reverse-transcribed into complementary DNA (cDNA) using the miRNA 1st Strand cDNA Synthesis Kit (by Stem-Loop) (MR101-01, Vazyme, China). Real-time PCR was performed using miRNA Universal SYBR qPCR Master Mix (MQ101-01, Vazyme, China) on a fast real-time PCR system (Thermo Fisher, USA). U6 was selected as the internal control. The primers for rno-miR-206–3p were as follows: forward primer: 5'-CCGCGTGGAAATGTAAGGAAGT-3'; reverse primer: 3'-AGTGCAGGGTCCGAGGTATT-5'; stem-loop primer: 5'-GTCGTATCCAGTGCAGGTCCGAGGTATTCCGAC.

TGGATACGACCCACAC-3'. The primers for U6 were as follows: forward primer: 5'-GCGCGTGCACCTATTTC-3'; reverse primer: 3'-AGTGCAGGGTCCGAGGTATT-5'; stem-loop primer: 5'-GTCGTATCCAGTGCAGGGTCCGAGGTATTCCGACTGGATACGA.

CTGCTTC-3'.

2.19. Statistical analysis

In this study, the data are presented as the mean \pm SD. Statistical analyses were carried out using GraphPad Prism software (version 8.0; San Diego, CA, USA). Comparisons of two groups were performed with Student's *t*-test, while one-way ANOVA followed by Tukey's correction was used for comparisons among multiple groups. Differences were considered statistically significant at *p* < 0.05.

3. Results

3.1. Preparation and characterizations of composite scaffolds

GC and DF-PEG were mixed to quickly form Schiff base linkages (Fig. 1A). Nanofiber (100 μ m in length) was fabricated by grinding in liquid nitrogen and high-speed pulverization (Fig. 1B). Then, composite scaffolds (mixture of the hydrogel and the nanofiber) loaded with BMSCs were administered intracranially into the perilesional site (Fig. 1C). An interconnected porous network structure of hydrogel, which was clearly observed by scanning electron microscope (SEM), greatly increased the surface area of the composite scaffold and enhanced the BMSCs-loading capacity (Fig. 1D).

The injectability of the composite scaffolds is shown in Fig. 1E. A newly formed hydrogel was observed at 4 h after injection. The hydrogel also showed self-adaptability, as it could change its morphology spontaneously and fuse together (Fig. 1F). The nanofiber was cut into short fibers (100 μ m in length) using a freezing microtome in Fig. 1G. The nanofiber was characterized by the core-shell-shaped nanostructure under TEM (Fig. 1H). The hydrophilic core-shell nanofiber was beneficial to cell adhesion and migration after plasma-treated (Fig. 1I).

The nanofiber was evenly dispersed in the hydrogel (Fig. 2A). In addition, unlike BMSCs grown in traditional adherent culture, BMSCs loaded in the composite scaffolds aggregated together and exhibited a sphere-like growth pattern (Fig. 2B), which indicated that these BMSCs may have great biological functions, especially powerful paracrine effects.

Then, the strain capacity and self-healing characteristics of the composite scaffolds were investigated. After mixing DF-PEG with GC solution, the storage modulus (*G'*) gradually increased, and it surpassed the loss modulus (*G''*) after approximately 60 s,

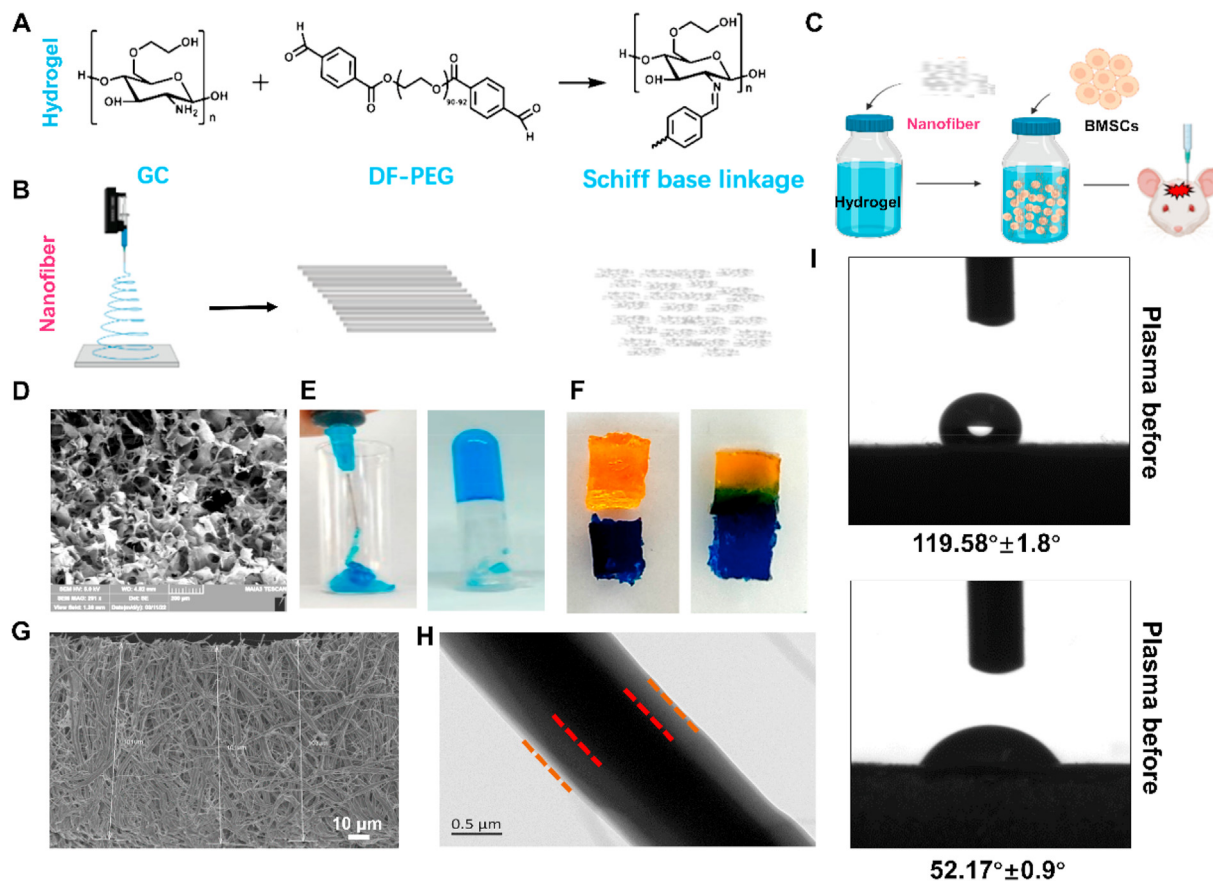


Fig. 1. Characterizations of the hydrogel and the nanofiber. (A) Hydrogel preparation through the formation of dynamic Schiff base linkages between GC and DF-PEG. (B) Nanofiber was prepared by grinding in liquid nitrogen and high-speed pulverization. (C) The procedure by which BMSCs were loaded in the composite scaffolds for cerebral ischemia treatment. (D) SEM image of the hydrogel. (E) The injectability and (F) self-adapting characteristics of the hydrogel. (G) SEM image of the nanofiber in 100 μm length. (H) TEM image of the nanofiber characterized by the core-shell nanostructure. (I) Schematic diagram between core-shell fibers and aqueous media.

suggesting the rapid formation of a cross-linked gel network (Fig. 2C). The mucoadhesive strength of the composite scaffolds was nearly 150–200 Pa (Fig. 2C), which indicated that the nanofibers in the composite scaffolds retained the characteristics of the hydrogel. Additionally, no obvious inflammatory cell infiltration was detected by hematoxylin and eosin (H&E) staining on day 1, 7, or 14 after subcutaneous injection of the composite scaffolds into the backs of rats (Fig. 2D), which indicated that the composite materials exhibited excellent biological safety.

3.2. The therapeutic effects of BMSCs loaded in composite scaffolds

Migration ability was assessed by the wound healing assay. Conditioned medium (CM) was harvested from cultured BMSCs and Scaffolds-loaded BMSCs. The results indicated that BMSCs cultured with BMSCs + Scaffolds-CM showed better migration ability than BMSCs cultured with BMSCs-CM (Fig. 3A and B; $p < 0.05$). Furthermore, under normal and OGD conditions, the BMSCs in the composite scaffolds group showed higher viability (Fig. 3C; $p < 0.001$) and stronger paracrine effects (BDNF and VEGF), suggesting the superior therapeutic potential of the scaffolds-loaded BMSCs in terms of neuroprotection, proangiogenesis, respectively, although there were no significant differences in IGF-1 levels under normal or OGD conditions (Fig. 3D, E, 3F; $p < 0.001$).

In addition, under OGD conditions, the number of live SH-SY5Y cells (Fig. 4A), the viability of SH-SY5Y cells (Fig. 4B; $p < 0.001$), SH-

SY5Y cell migration (Fig. 4C and D; $p < 0.01$), average neurite outgrowth (Fig. 4E and F; $p < 0.01$), and the angiogenic capacity of HUVECs (Fig. 4G and H; $p < 0.001$) were markedly increased in the group treated with BMSCs + Scaffolds-CM than in the group treated with BMSCs-CM and the group treated with control medium.

3.3. Composite scaffolds improved BMSCs retention in the brain

After transplantation, stronger BMSCs bioluminescence was observed in the MCAO + BMSCs + Scaffolds group than in the MCAO + BMSCs group, and there was a clear bioluminescence signal in the MCAO + BMSCs + Scaffolds group even at 14 days. This result indicated that the composite scaffolds could improve BMSCs retention in the brain (Fig. 5A and B).

Additionally, the number of RFP-positive cells in the MCAO + BMSCs group decreased rapidly. In contrast, BMSCs loaded in composite scaffolds not only maintained a strong RFP signal but also tended to be dispersed, which suggested that these cells could dynamically migrate into the injured area of the brain (Fig. 5C).

3.4. BMSCs loaded in composite scaffolds alleviated ischemic injury

There is the scheme in animal to assess the therapeutic potential of scaffolds-loaded BMSCs (Fig. 6A). At 7 days after MCAO, the infarct area was significantly reduced (Fig. 6B and C; $p < 0.01$) and brain edema was attenuated (Fig. 6D; $p < 0.01$) in the

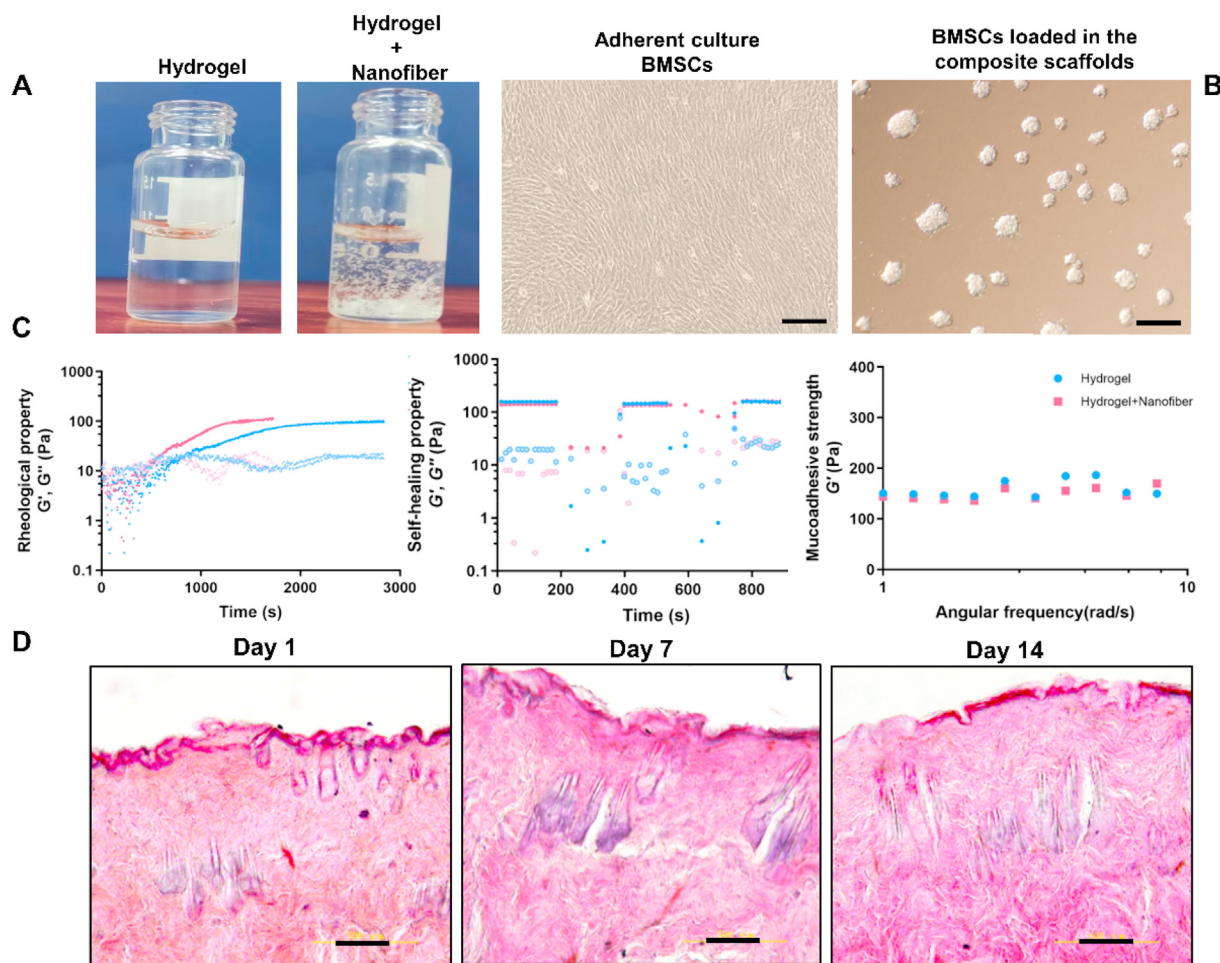


Fig. 2. Characterizations and biosafety of the composite scaffolds. (A) The nanofiber was evenly dispersed in the hydrogel. (B) Morphology of BMSCs loaded in the composite scaffolds. (C) Analyses of the rheological properties, self-healing properties, and mucoadhesive strength of the hydrogel and hydrogel + nanofiber composite scaffolds. (D) Biosafety analysis of the composite scaffolds following subcutaneous injection into the backs of rats by using HE staining, scale bars = 250 μm .

MCAO + BMSCs group at 3 days after MCAO, compared with the MCAO + BMSCs group. In addition, at both 7 days and 14 days after MCAO, neurological deficits were significantly ameliorated in the animals treated with BMSCs loaded in composite scaffolds compared with those in the MCAO + BMSCs group (Fig. 6E, F and 6G).

The numbers of Iba-1-positive cells (Fig. 7B; $p < 0.01$) at 3 days after MCAO, and activated astrocytes (Fig. 7E; $p < 0.01$) at 14 days after MCAO were significantly decreased in the MCAO + BMSCs + Scaffolds group compared with the MCAO + BMSCs group. Additionally, BMSCs loaded in composite scaffolds increased the number of Nestin-positive cells (Fig. 7C; $p < 0.01$) and CD31 neovascularization (Fig. 7D; $p < 0.01$) within the ischemic penumbra in the brain.

3.5. BMSCs loaded in composite scaffolds activated the PI3K/AKT signaling pathway

Fig. 8A and B shows that almost all of the DEPs were enriched in the cytoplasm and the cell membrane. Fig. 8B shows that 1313,39.55% of the differentially expressed proteins were located in the cytoplasm, while 911,27.44% were located in the membrane.

These percentages were dramatically different from those shown in Fig. 8A (cytoplasm: 90, 35.02%; membrane: 70, 27.24%). GO enrichment analysis showed that the DEPs were enriched in "regulation of cellular protein metabolism process (Fig. 8C). KEGG pathway analysis showed that the DEPs were also enriched in to the "phosphatidylinositol pathway" and "oxidative phosphorylation process", as shown (Fig. 8F). Wiki pathway analysis showed that the DEPs were enriched in "PI3K/AKT signaling", "G protein signaling pathways" and "oxidative phosphorylation", as shown in Fig. 8G and H.

These enrichment analyses indicated that signaling pathways associated with tissue growth, repair, and regeneration might play essential roles in the chronic phase of ischemic stroke. The PI3K/AKT signaling pathway is the main pathway involved in phosphatidylinositol signaling [21]. In addition, VEGFR2 and VEGFA, which are involved in angiogenesis, and cleaved caspase-3, which is associated with the neuronal apoptotic cascade, are downstream proteins of the PI3K/AKT signaling pathway [22,23].

As shown in Fig. 8I, the levels of p-PI3K and p-AKT were markedly reduced after MCAO, and these changes were reversed by BMSCs treatment, especially treatment with scaffolds-loaded BMSCs. Furthermore, the expression levels of VEGFR2 and VEGFA

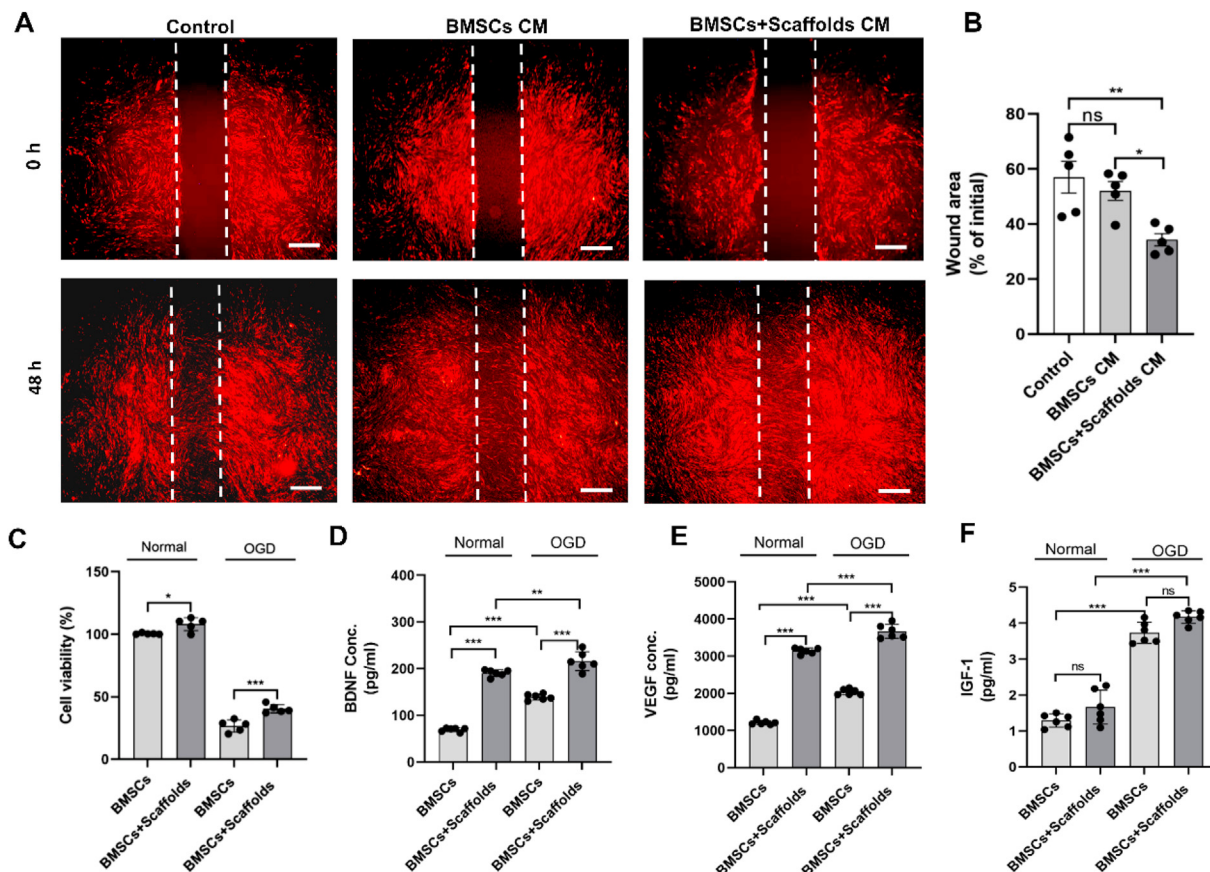


Fig. 3. Scaffolds-loaded BMSCs showed stronger biological effects. The effects of suspended BMSCs- and BMSCs + Scaffolds-derived CM on BMSCs migration (A and B) and BMSCs viability (C) under normal and OGD conditions. (D–F) The concentrations of paracrine factors in BMSCs- and BMSCs + Scaffolds-CM under normal and OGD conditions. The data are presented as the mean ± SEM. Student's *t*-test was used to analyze the data in D–F, while one-way ANOVA followed by Tukey's post hoc test was used to analyze the data in B and C. **p* < 0.05; ***p* < 0.01; ****p* < 0.001; ns, not significant.

were significantly increased and the level of cleaved caspase-3 was markedly decreased in the MCAO + BMSCs + Scaffolds group compared with the MCAO + BMSCs group.

3.6. Differential expression analysis of miRNAs confirmed that the effect of scaffold-loaded BMSCs was strongly associated with the PI3K/AKT signaling pathway

Exosomes extracted from the BMSCs-CM group and BMSCs + Scaffolds-CM group appeared as typical spherical structures covering the biofilm (Fig. 9A). The average particle size of the exosomes was almost 60–120 nm (Fig. 9B). Nano FCM revealed the expression of the specific markers CD9, CD63, and CD81 on the exosomes (Fig. 9C).

DE miRNAs were further analyzed, and GO enrichment, KEGG pathway, and Reactome enrichment analysis revealed that the predicted DE miRNAs were enriched in the PI3K/AKT signaling pathway (Fig. 9D–F). GO enrichment analysis revealed that the differentially expressed miRNAs were related to “positive regulation of protein serine/threonine kinase activity” (Fig. 9D). KEGG analysis showed that the differentially expressed miRNAs were enriched in the “PI3K/AKT signaling pathway” (Fig. 9E). Reactome enrichment analysis indicated that the differentially expressed miRNAs were associated with “signaling by receptor tyrosine

kinase” (Fig. 9F). These results implied that the mechanism underlying the reparative effects of composite scaffolds-loaded BMSCs in was strongly related to the PI3K/AKT signaling pathway.

3.7. Lower expression of miR-206–3p in composite scaffolds-loaded BMSCs enhanced the activity of the PI3K/AKT signaling pathway

The volcano plot showed that there were 11 upregulated miRNAs and 11 downregulated miRNAs (Fig. 10A). The heatmap (Fig. 10B) and column diagram (Fig. 10C) show that miR-206–3p was significantly differentially expressed in BMSCs-derived exosomes vs. BMSCs + Scaffolds-derived exosomes. The miR-206–3p expression level was verified by RT-PCR (Fig. 10D; *p* < 0.01). The results of differential expression analysis (Fig. 10A–C) and enrichment analysis of the differentially expressed miRNAs (Fig. 9D–F) indicated that miR-206–3p may be strongly associated with the PI3K/AKT signaling pathway. Then, the binding sites between miR-206–3p and the PI3K gene were predicted by utilizing the miRWalk database (<http://mirwalk.umm.uni-heidelberg.de>) (Fig. 10F), and the binding sites for the sequences 1394–1412 of the PI3K gene were validated by a dual-luciferase reporter gene assay (Fig. 10E; *p* < 0.01).

Furthermore, the expression levels of PI3K/AKT signaling pathway-related proteins were measured following transfection of

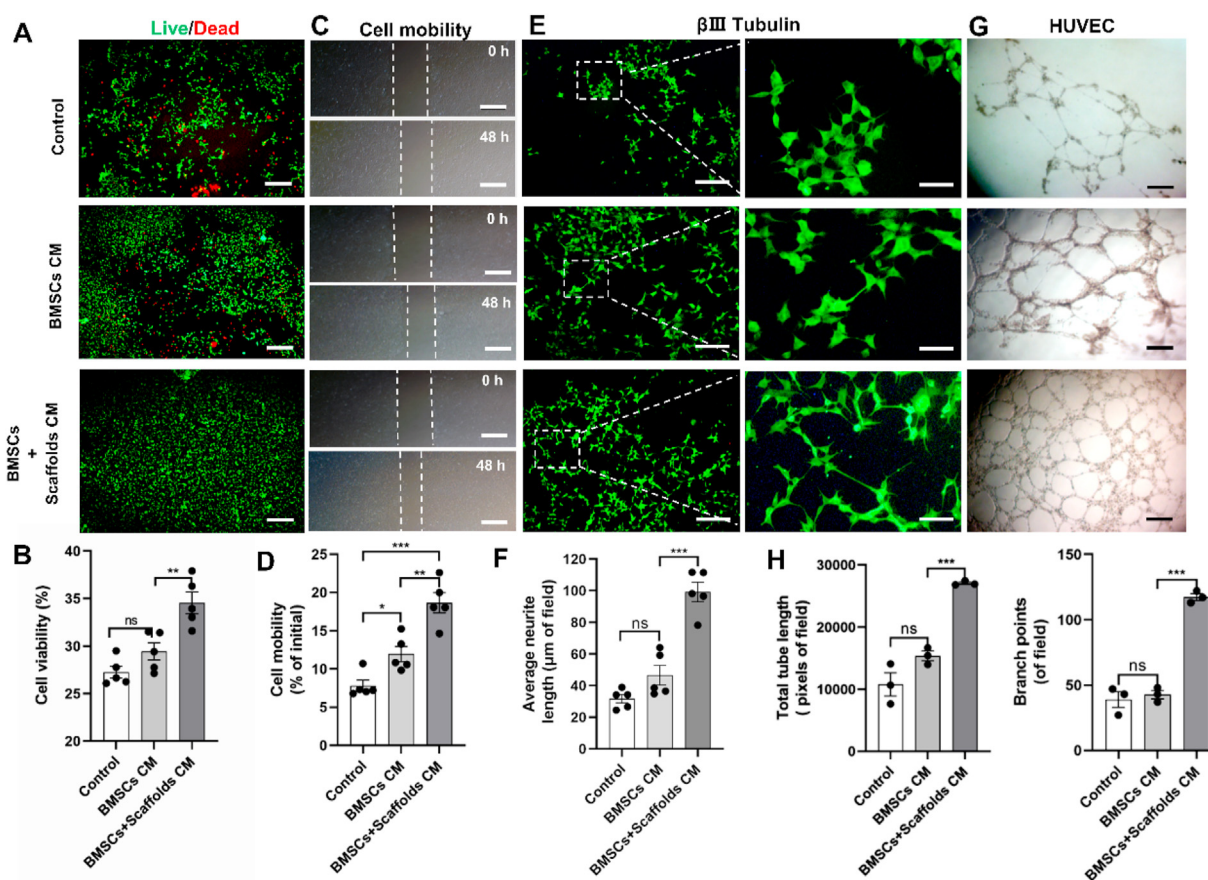


Fig. 4. Neuroprotective and angiogenic effects of scaffolds-loaded BMSCs under OGD conditions. The effects of BMSCs- and BMSCs + Scaffolds-CM on the SH-SY5Y cells viability (A and B) and migration (C and D) of neuroblasts under OGD conditions; scale bars = 500 μm. (E, F) The average neurite length was evaluated; scale bars = 250 μm (left) and 50 μm (right). (G) The angiogenic ability HUVECs treated with BMSCs-CM or BMSCs + Scaffolds-CM was tested; scale bars = 500 μm. (H) The number of branch points and number of total tubes were markedly increased in the BMSCs + Scaffolds-derived CM group compared with the other groups. ****p* < 0.001, compared with HUVECs treated with BMSCs-CM. The data are presented as the mean ± SEM. For B–H, all *p* values were determined by one-way ANOVA followed by Tukey's post hoc test. **p* < 0.05; ***p* < 0.01; ****p* < 0.001; ns, not significant.

the miR-206–3p agomir, and antagomir. The miR-206–3p agomir, agomir-NC, antagomir, and antagomir-NC respectively transfected into BMSCs to modulate the expression of miR-206–3p to further determine whether miR-206–3p was responsible for alterations in the expression of PI3K/AKT signaling pathway-related proteins.

As shown in Fig. 10G and H, the expression of p-PI3K/p-AKT and its downstream proteins VEGFR2 and VEGFA was upregulated after miR-206–3p antagomir treatment (MCAO + BMSCs group) and downregulated following miR-206–3p agomir treatment (MCAO + BMSCs + Scaffolds group). Conversely, the cleaved caspase-3 showed the opposite trend. These results indicate that miR-206–3p could negatively modulate the expression of PI3K/AKT signaling pathway proteins and the activity of the PI3K/AKT signaling pathway. Therefore, the neuroprotective and angiogenic effects of scaffolds-loaded BMSCs might be at least partly mediated by suppressing miR-206–3p expression and enhancing the activity of the PI3K/AKT signaling pathway.

4. Discussion

In this study, we developed composite scaffolds comprising self-adapting, injectable hydrogel and nanofiber, which mimicked the natural extracellular matrix (ECM) in the brain. These scaffolds protected transplanted BMSCs from an unfavorable ischemic

microenvironment and effectively reduced BMSCs loss in the injection area. The *in vivo* study indicated that BMSCs loaded in the composite scaffolds might exert their neuroprotective effects by downregulating miR-206–3p expression in exosomes and consequently enhancing the activity of the PI3K/AKT signaling pathway.

Nowadays, a still difficult problem is how to maintain the transplanted stem cells, biological activities and functions. One effective solution is to incorporate stem cells into a relevant protective biomaterials. Hydrogel, owing to the similarity and favorite biological compatibility to ECM, is a promising candidate for stem cells transplanted [24]. We know that the two main and abundant ECM components are proteoglycan hydrogels and nanofibrous proteins [25], which is a major goal for mimicking the biomechanical characteristics of the native tissue in tissue engineering. Electrospun materials, due to their nanofibrous structure, also are promising tissue engineering biomaterials, and have been reported to enhance cell outgrowth, attachment, proliferation, and differentiation [26,27].

In this study, we adopt the composite scaffolds for the self-adopting hydrogel based on the Schiff linkage and the nanofiber based on the GelMA as the core polymer, PCL as the shell polymer. As the cells carrier, the composite scaffolds can protect the embedded stem cells from being dispersed and death, due to the missing of anchorage to matrix, known as anoikis [28–32], and

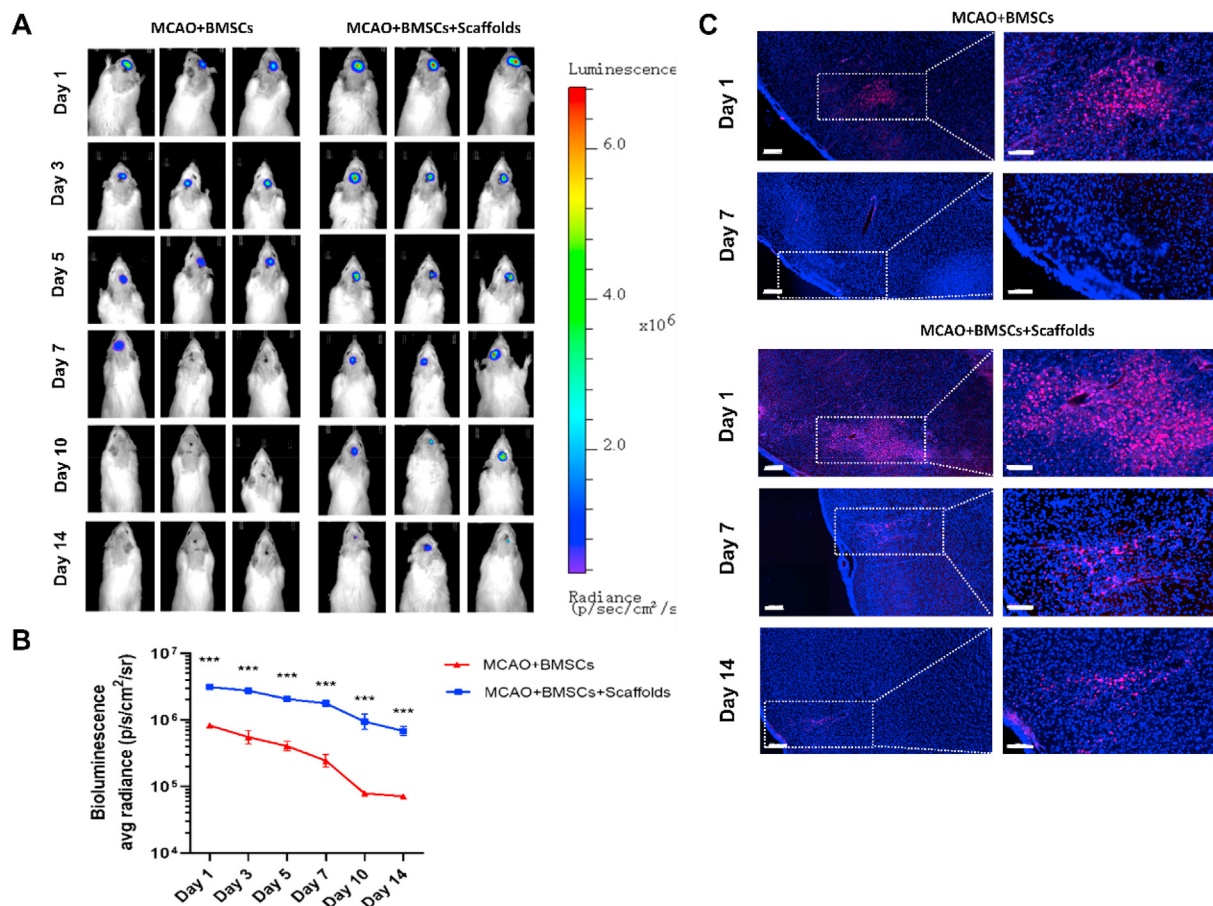


Fig. 5. BMSCs loaded in composite scaffolds exhibited prolonged retention in the brain. (A) and (B) The brain retention of BMSCs in each group was evaluated by IVIS imaging. IVIS images of BMSCs and scaffolds-loaded BMSCs in MCAO rats were obtained at 1 d, 3 d, 5 d, 7 d, 10 d, and 14 d. (C) The bioluminescence signal intensities of transplanted BMSCs or scaffolds-loaded BMSCs (stably expressing RFP) in MCAO rats were determined; scale bars = 200 μm (left) and 100 μm (right). The retention period of BMSCs loaded in composite scaffolds was much longer than that of BMSCs in the saline group. The data are presented as the mean \pm SEM. Student's *t*-test was used to determine *p* values. ****p* < 0.001 vs. the MCAO + BMSCs group.

maintain high concentrated stem cells at the injection sites to enhance the therapeutic potential [32]. Moreover, the embedded stem cells can regulate their morphology, migration, and spread [33].

Although extensive basic research on ischemic stroke has been performed, little progress has been made in clinical therapy. Currently, much attention is paid to relieving symptoms and promoting long-term functional recovery. Therefore, research on novel therapeutic strategies has focused on treatments that facilitate neural regeneration and angiogenesis following ischemic stroke. Although BMSCs have exhibited enhanced tissue and vascular repair capacities in some brain disorders, some key challenges, e.g., poor stem cell survival in local brain areas after transplantation, need to be overcome to maximize the efficacy of BMSCs treatment [34]. Engineered biomaterial scaffolds loaded with stem cells have been shown to be a novel and promising strategy for ischemic stroke [2,3]. In this study, we first tested the characteristics of the composite scaffolds. The excellent BMSCs-loading capacity, injectability, and histocompatibility of the scaffolds indicated their application potential. Furthermore, the retention period of the composite scaffolds-loaded BMSCs loaded within local brain areas was significantly extended, which implied that the cavities and nanofibers within the composite scaffolds could protect the BMSCs

from degradation or elimination by the brain immune system and that BMSCs could exert their effects for a prolonged period of time in the ischemic microenvironment.

In addition, BMSCs loaded in composite scaffolds retained migration capacity and paracrine secretion ability, which may have allowed them to exert critical neuroprotective effects after ischemic stroke. This may have been because, compared with conventional two-dimensional monolayered culture, the three-dimensional stereoscopic culture provided by composite scaffolds could effectively increase intercellular interactions [3,35] and enhance the release of extracellular vesicles and exosomes [36,37].

There are some hypotheses about the neuroprotective mechanism of BMSCs transplantation, such as the transformation and paracrine secretion theories [38–40]. In this study, conditioned medium from BMSCs evidently promoted angiogenesis and neural regeneration following MCAO, which indicated that BMSCs exerted their effects at least partly through their paracrine secretion function and that the conditioned medium contained important neurotrophic or angiogenic factors.

After cerebral ischemia, the infarct volume, extent of brain edema, and neurological deficits were significantly reduced by BMSCs treatment, especially by BMSCs loaded in composite scaffolds, which implied that dysfunction of the NVU (neurovascular

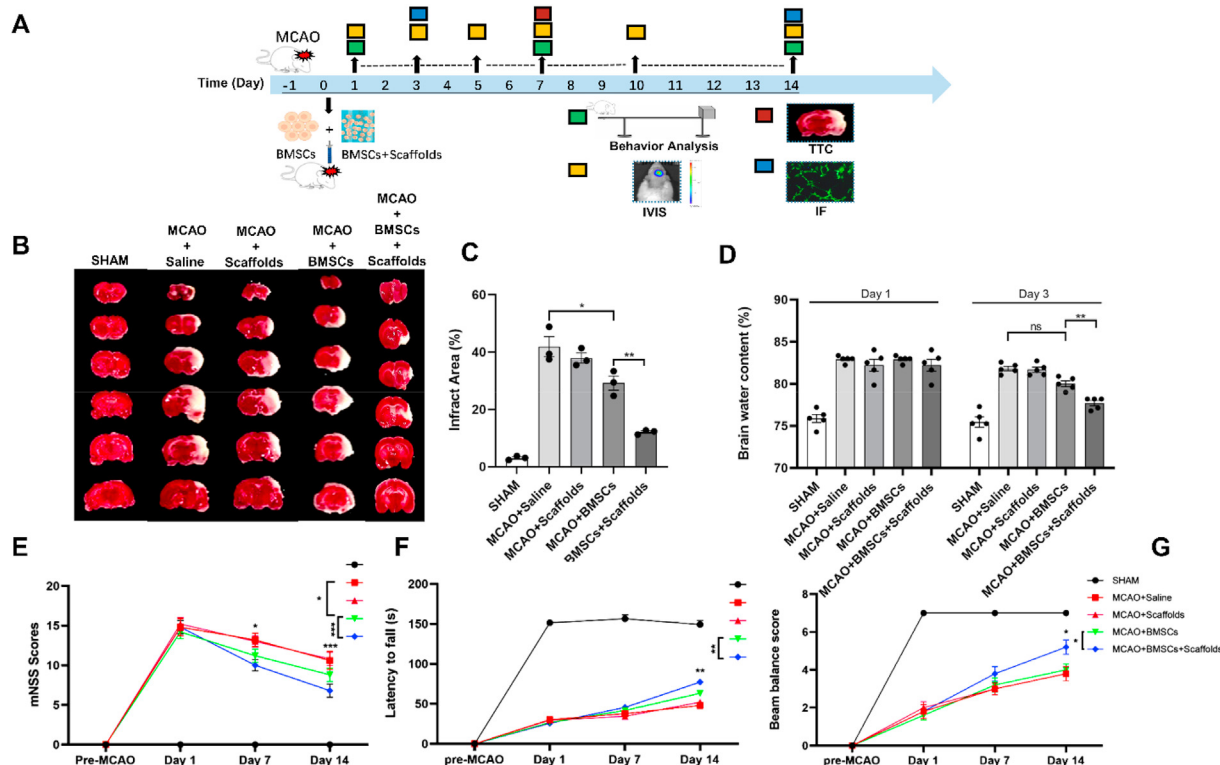


Fig. 6. BMSCs loaded in composite scaffolds ameliorated ischemic stroke. (A) Scheme of the *in vivo* experiment. (B, C) The effects of BMSCs and scaffolds-loaded BMSCs were assessed by TTC staining. (D) The brain water content at 1 d and 3 d post-MCAO. Motor function recovery in MCAO model rats was assessed with (E) mNSS scores, the rotarod test (F), and beam balance analysis (G). The data are presented as the mean \pm SEM. For C-G, all *p* values were determined by one-way ANOVA followed by Tukey's post hoc test. **p* < 0.05; ***p* < 0.01; ****p* < 0.001; ns, not significant.

unit, NVU) within the penumbra was attenuated. To assess the effects of BMSCs treatment on glial cells, the activities of microglia and astrocytes were evaluated. Following MCAO, microglia and astrocytes in the brain are overactivated due to stimulation by various harmful factors, leading to extensive cytokine production and glial scar formation. In the present study, the overactivation of microglia in the penumbra was dramatically suppressed by the transplantation of BMSCs loaded in composite scaffolds. These results implied that neuroinflammation in the brain was markedly reduced. In addition, the expression level of GFAP in astrocyte was decreased, which reduced the formation of the glial scar and facilitated neural regeneration following ischemic insult. Our results were in accordance with previous results showing that MSCs can effectively decrease glial scarring following ischemic brain injury [41].

Given the enhanced protective effects of BMSCs loaded in composite scaffolds, we explored the potential mechanism. Proteomics analysis revealed that PI3K/AKT signaling pathway activation was dramatically different among the groups; additionally, exosome sequencing analysis revealed that the differentially expressed genes were enriched in pathways involved in the PI3K/AKT signaling pathway. The PI3K/AKT signaling pathway has critical functions in promoting cell proliferation, tissue restoration and regeneration and inhibiting apoptosis [42]. Western blotting results confirmed that the expression of PI3K/AKT signaling-related proteins and downstream target proteins, such as VEGFR2 and VEGFA, were enhanced.

Many studies have focused on the vascular and neural regeneration effects of MSC-derived exosomes [43,44]. MicroRNAs

(miRNAs) play pivotal roles in exosome functions. miRNAs are endogenous small noncoding RNAs that play critical roles in pathological processes and biological effects, such as in cancer, heart diseases, and neurological disorders [45–47]. In the present study, miRNA sequencing revealed that the expression of miR-206–3p (an isoform of miR-206) was dramatically different in the presence and absence of composite scaffolds. miR-206–3p is an isoform of miR-206 and may play a vital role in the CNS [12]. Therefore, we hypothesized that miR-206–3p might be involved in regulating the PI3K/AKT signaling pathway after BMSCs or BMSCs + Scaffolds treatment. By using a dual-luciferase reporter assay, we confirmed that miR-206–3p could bind to the 1394–1412 region of the PI3K gene. After ischemic injury, overexpression of miR-206–3p markedly suppressed the activity of the PI3K/AKT signaling pathway, which led to brain injury. After BMSCs treatment, especially treatment with composite scaffolds-loaded BMSCs, the level of miR-206–3p was significantly decreased, its inhibitory effects on the PI3K/AKT signaling pathway were reduced, and ischemic brain injury was alleviated.

In summary, these observations implied that the proangiogenic and neuroprotective potentials of hydrogel/nanofiber composite scaffolds loaded with BMSCs were related to the effect of miR-206–3p on the PI3K/AKT signaling pathway after ischemic insult (Fig. 11).

Although we successfully developed novel and promising hydrogel/nanofiber composite scaffolds with marked therapeutic potential for ischemic stroke, several limitations must be addressed before these scaffolds can be used in the clinic. First, in this study, to bypass the blood–brain barrier, the scaffolds-loaded BMSCs were

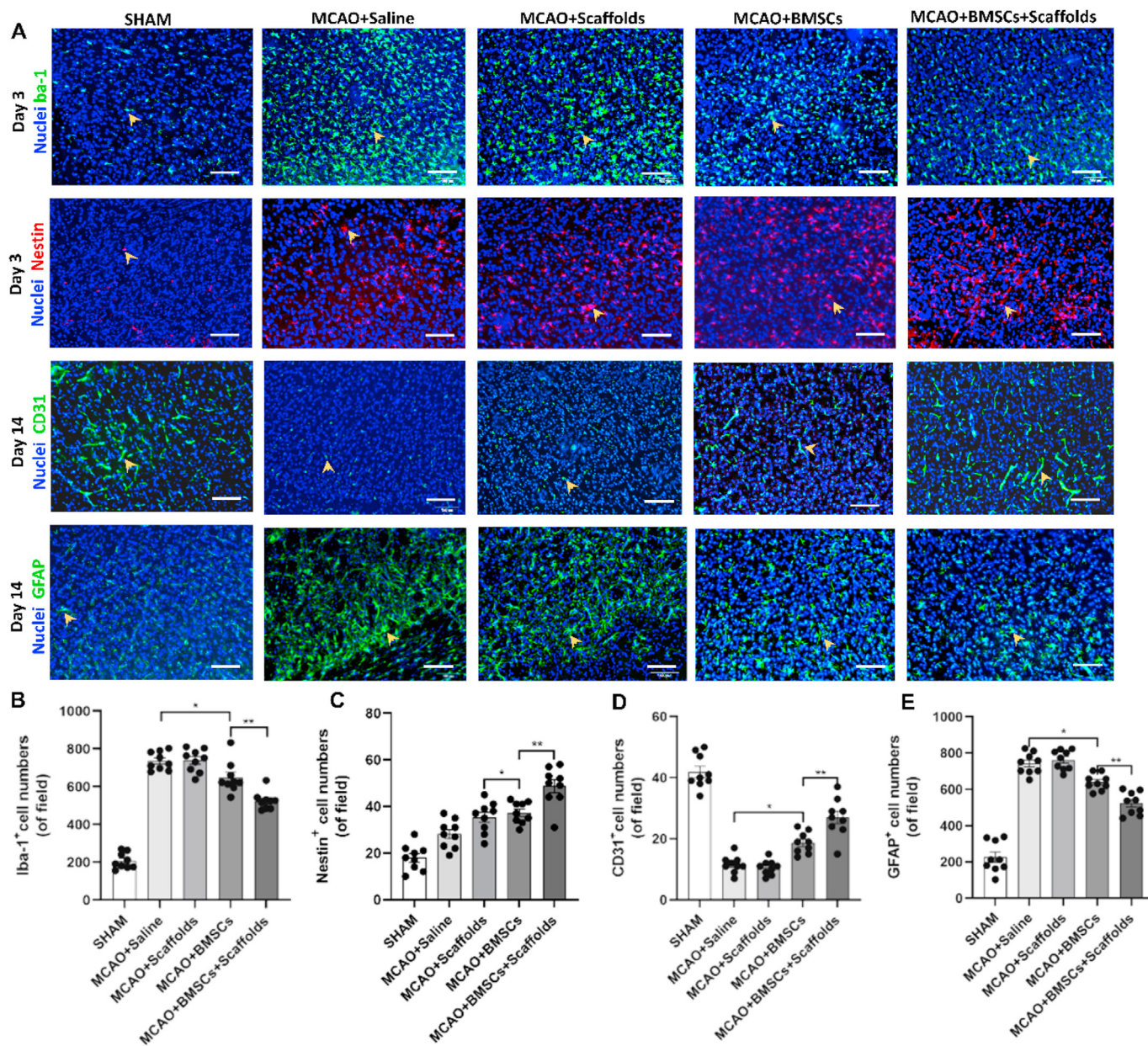


Fig. 7. BMSCs loaded in composite scaffolds enhanced neurogenesis and angiogenesis after MCAO. (A) Fluorescence images of microglial cells (Iba-1) and neural stem cells (Nestin) at 3 days after MCAO and vascular endothelial cells (CD31), astrocytes (GFAP) at 14 days post-MCAO. (B–E) Quantitative analysis of Iba-1⁺, Nestin⁺, CD31⁺ and GFAP⁺ expression; scale bars = 250 μm. At 3 days after MCAO, the expression of Iba-1 was significantly decreased in the MCAO + BMSCs + Scaffolds group (B), and neurogenesis (C) and angiogenesis (D) were markedly increased. The number of GFAP-positive cells was significantly reduced after scaffolds-loaded BMSCs treatment (E). The data are presented as the mean ± SEM. For (B–E), *p* values were determined by one-way ANOVA followed by Tukey's post hoc test. **p* < 0.05; ***p* < 0.01; ns, not significant.

administered by stereotactic injection. This method might result in increased intracranial pressure and tissue swelling, which is not favorable for clinical patients. To guarantee patient safety, optimized transplantation approaches for stem cell treatment are urgently needed. Second, the biosafety of the nanofiber/hydrogel material must be further explored and evaluated, as the properties of the materials might change before and after solidification. Last, precise identification of the optimal transplantation window during ischemic pathology is critical for ensuring the efficacy and safety of stem cell transplantation.

5. Conclusion

In summary, in this study, we reported the protective effects of BMSCs loaded in novel nanofiber/hydrogel composite scaffolds on brain injury after ischemic insult. These composite scaffolds-loaded BMSCs might exert their effects by modulating the inhibitory action of miR-206-3p on the PI3K/AKT signaling pathway. Due to its ability to enhance angiogenesis and neural regeneration in the penumbra, the BMSCs/nanofiber/hydrogel composite scaffolds system could be a potential therapeutic strategy for the clinical treatment of ischemic brain injury.

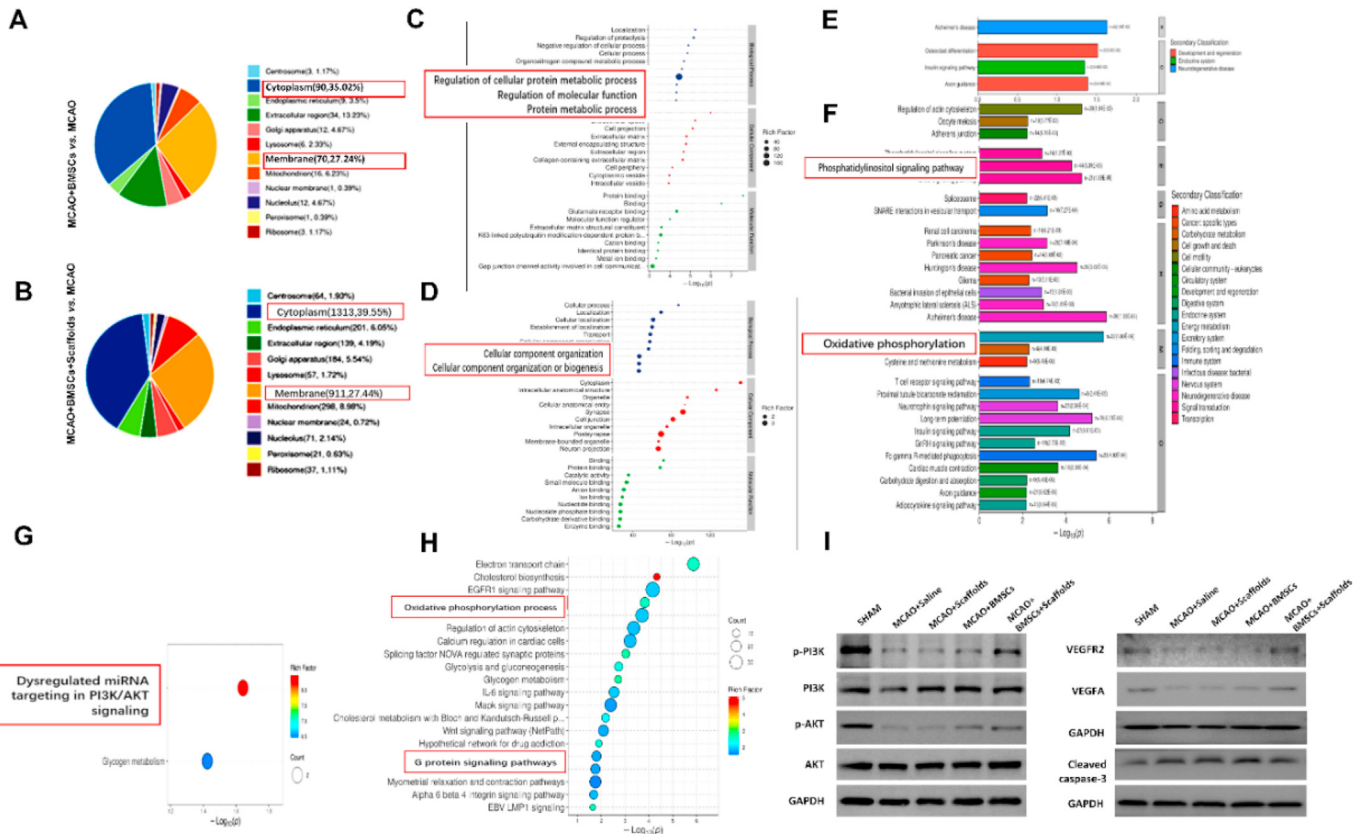


Fig. 8. BMSCs loaded in composite scaffolds ameliorated ischemic brain injury by promoting the PI3K/AKT signaling pathway. (A) and (B) Enrichment analysis showing the subcellular localization of the DEPs. (C) and (D) GO enrichment, (E) and (F) KEGG pathway, (G) and (H) Wiki pathway analyses of DEPs in the MCAO + BMSCs group vs. MCAO group and the MCAO + BMSCs + Scaffolds group vs. MCAO group. (I) The differential expression levels of PI3K/AKT signaling pathway-related and downstream proteins among the groups were confirmed by western blotting analysis.

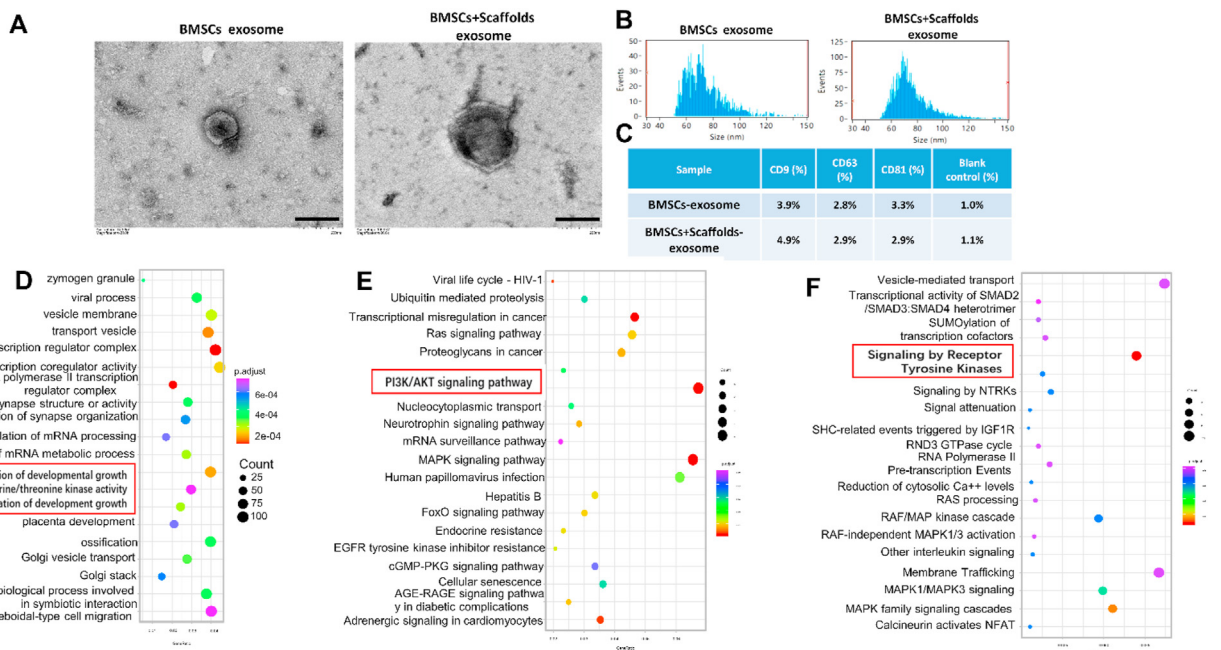


Fig. 9. Extraction and identification of exosomes and high-throughput sequencing of miRNAs. (A) Visualization of exosomes derived from the two groups under TEM; scale bar = 100 nm. (B) The average particle size of the exosomes derived from the two group was 60–120 nm. (C) The expression of the specific markers CD9, CD63, and CD81 on the exosomes. (D), (E), and (F) GO enrichment, KEGG pathway, and Reactome enrichment analyses and high-throughput sequencing of the differentially expressed miRNAs in the two groups.

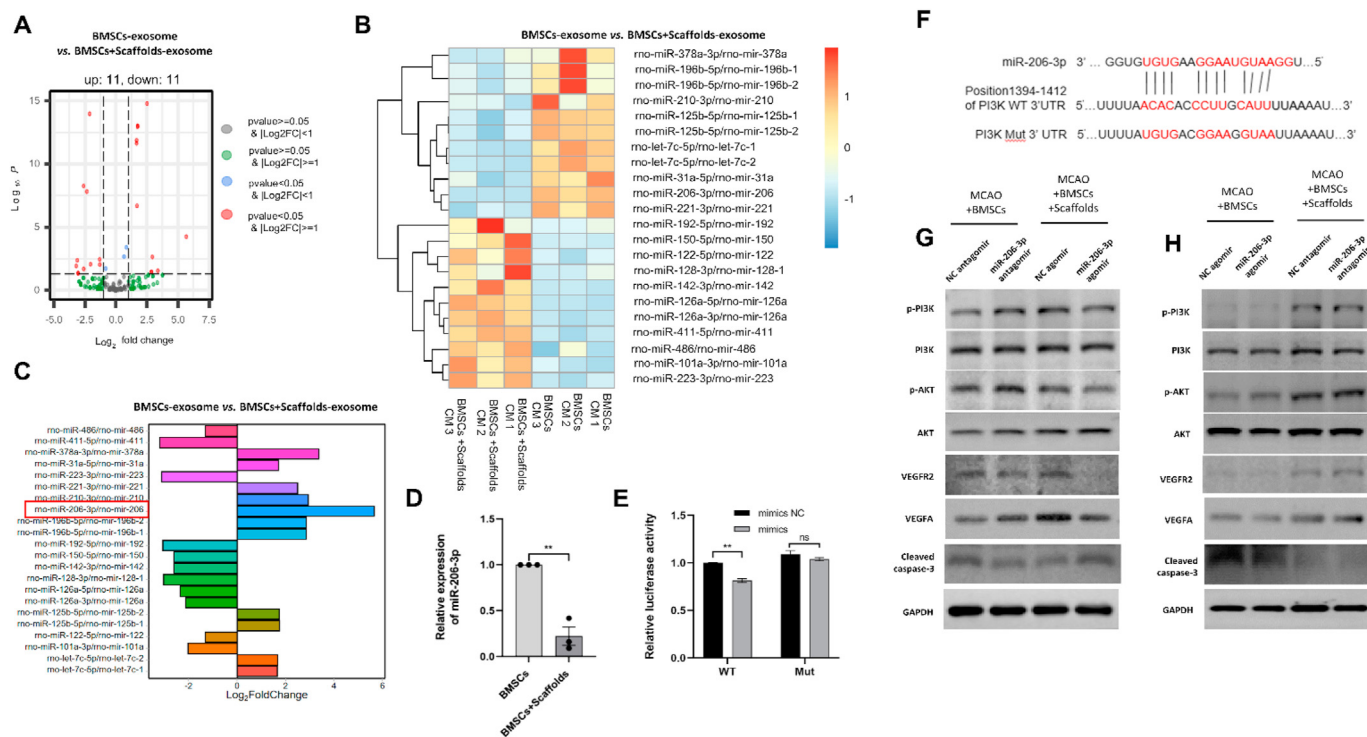


Fig. 10. Lower expression of miR-206–3p in BMSCs + Scaffolds-derived exosomes ameliorated ischemic stroke by inhibiting the degradation of PI3K. (A–C) A volcano plot, heatmap, and column diagram showing differentially expressed miRNAs between the BMSCs-exosome group and the BMSCs + Scaffolds-exosome group. (D) Differential miR-206–3p expression between exosomes derived from the two groups was verified by RT-PCR. (E, F) The binding sites between miR-206–3p and the PI3K gene predicted by the miRWalk database and verified by a dual luciferase reporter gene assay. (G, H) Western blotting analysis was used to validate differential protein expression between the MCAO + BMSCs group and MCAO + BMSCs + Scaffolds group after transfection with miR-206–3p agomir or antagomir. The data are presented as the mean ± SEM. Student’s *t*-test was used to analyze the data for (D), while one-way ANOVA with Tukey’s post hoc test was used to analyze the data in E. *****p* < 0.01**; ns, not significant.

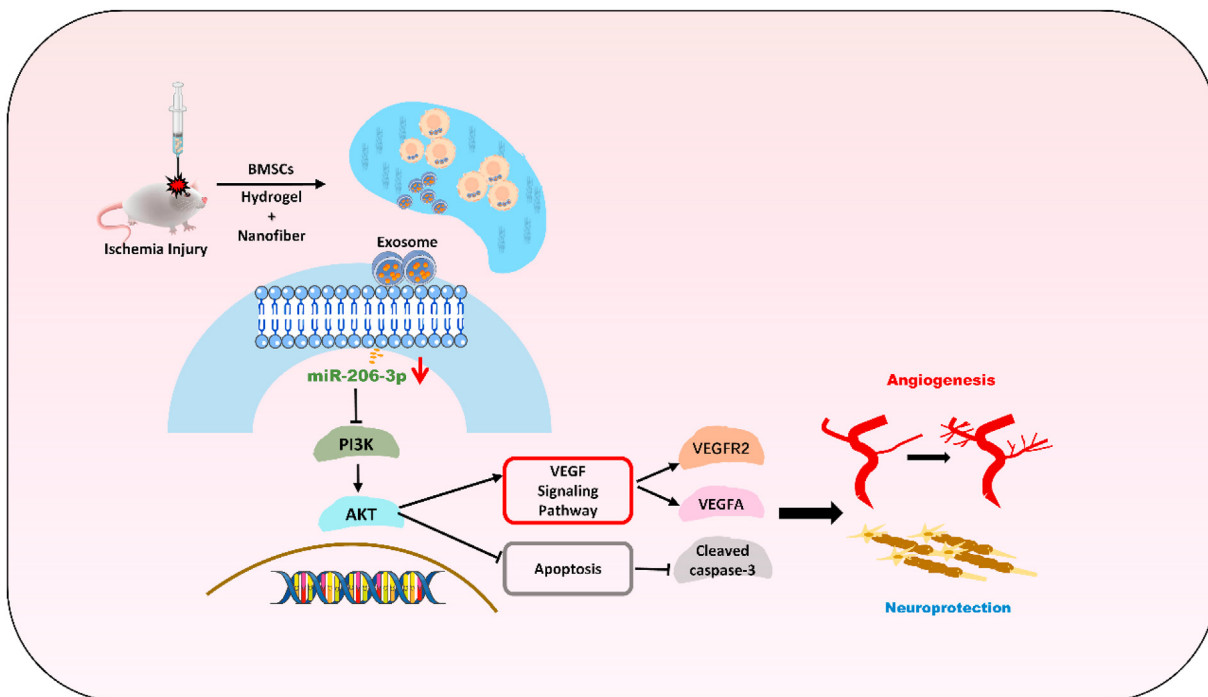


Fig. 11. BMSCs in hydrogel/nanofiber composite scaffolds have a better effect for angiogenesis and neuroprotection after ischemic brain injury through enhancing PI3K/AKT signaling pathway activity via suppressing miR-206–3p expression.

Credit author statement

Yanhong Pei designed the research, performed experiments, analyzed the data, and wrote the manuscript. Junhao Yan designed, supervised the research, and wrote the manuscript. Hongquan Zhang supervised the research. Xing Wang provided the hydrogel. Lifei Huang provided the properties of the hydrogel and the nanofiber. Jiajia Xue provided the nanofiber. Tong Wang provided the flow chart of the fabrication of nanofiber. Qinhan Yao assisted with the BMSCs isolation. Yanrong Sun assisted with cell culture. Yan Zhang assisted with RT-PCR experiment. Xiaomei Yang assisted with frozen sections preparation. Jiliang Zhai and Lihua Qin assisted with western blotting analysis.

Declaration of competing interest

The authors declare that they have no known competing financial interests or personal relationships that could have appeared to influence the work reported in this paper.

Data availability

The authors do not have permission to share data.

Acknowledgements

This study was supported by grants from the Beijing Natural Science Foundation (grant Z200025), supporting Platform Construction Project of Peking University Health Science Center (No. BMU2021ZC011) to Junhao Yan, and the grants from the National Natural Science Foundation of China (No. 81873818, 82171635).

References

- [1] C.L. Gibson, Cerebral ischemic stroke: is gender important? *J. Cerebr. Blood Flow Metabol.* 33 (9) (2013) 1355–1361.
- [2] B. Zhang, W. Yan, Y. Zhu, W. Yang, W. Le, B. Chen, R. Zhu, L. Cheng, Nano-materials in neural-stem-cell-mediated regenerative medicine: imaging and treatment of neurological diseases, *Adv. Mater.* 30 (17) (2018), e1705694.
- [3] Y. Petrenko, E. Sykova, S. Kubinova, The therapeutic potential of three-dimensional multipotent mesenchymal stromal cell spheroids, *Stem Cell Res. Ther.* 8 (1) (2017) 94.
- [4] Y.H. Tang, Y.Y. Ma, Z.J. Zhang, Y.T. Wang, G.Y. Yang, Opportunities and challenges: stem cell-based therapy for the treatment of ischemic stroke, *CNS Neurosci. Ther.* 21 (4) (2015) 337–347.
- [5] J. Wang, W. Yang, H. Xie, Y. Song, Y. Li, L. Wang, Ischemic stroke and repair: current trends in research and tissue engineering treatments, *Regen Med Res* 2 (1) (2014) 3.
- [6] K.F. Bruggeman, Y. Wang, F.L. Maclean, C.L. Parish, R.J. Williams, D.R. Nisbet, Temporally controlled growth factor delivery from a self-assembling peptide hydrogel and electrospun nanofiber composite scaffold, *Nanoscale* 9 (36) (2017) 13661–13669.
- [7] X. Yuan, X. Wang, C. Chen, J. Zhou, M. Han, Bone mesenchymal stem cells ameliorate ischemia/reperfusion-induced damage in renal epithelial cells via microRNA-223, *Stem Cell Res. Ther.* 8 (1) (2017) 146.
- [8] J.J. Chen, S.H. Zhou, Mesenchymal stem cells overexpressing MiR-126 enhance ischemic angiogenesis via the AKT/ERK-related pathway, *Cardiol. J.* 18 (6) (2011) 675–681.
- [9] B.P. Hung, J.N. Harvestine, A.M. Saiz, T. Gonzalez-Fernandez, D.E. Sahar, M.L. Weiss, J.K. Leach, Defining hydrogel properties to instruct lineage- and cell-specific mesenchymal differentiation, *Biomaterials* 189 (2019) 1–10.
- [10] K. Zhang, L. Yu, F.R. Li, X. Li, Z. Wang, X. Zou, C. Zhang, K. Lv, B. Zhou, S. Mitragotri, M. Chen, Topical application of exosomes derived from human umbilical cord mesenchymal stem cells in combination with sponge spicules for treatment of photoaging, *Int. J. Nanomed.* 15 (2020) 2859–2872.
- [11] G. Ma, Y. Wang, Y. Li, L. Cui, Y. Zhao, B. Zhao, K. Li, MiR-206, a key modulator of skeletal muscle development and disease, *Int. J. Biol. Sci.* 11 (3) (2015) 345–352.
- [12] W. Guan, D.W. Xu, C.H. Ji, C.N. Wang, Y. Liu, W.Q. Tang, J.H. Gu, Y.M. Chen, J. Huang, J.F. Liu, B. Jiang, Hippocampal miR-206-3p participates in the pathogenesis of depression via regulating the expression of BDNF, *Pharmacol. Res.* 174 (2021), 105932.
- [13] N. Tian, Z. Cao, Y. Zhang, MiR-206 decreases brain-derived neurotrophic factor levels in a transgenic mouse model of Alzheimer's disease, *Neurosci. Bull.* 30 (2) (2014) 191–197.
- [14] P.L. Hung, M.H. Hsu, H.R. Yu, K.L.H. Wu, F.S. Wang, Thyroxin protects white matter from hypoxic-ischemic insult in the immature Sprague(-)Dawley rat brain by regulating periventricular white matter and cortex BDNF and CREB pathways, *Int. J. Mol. Sci.* 19 (9) (2018).
- [15] N. Cormier, A. Yeo, E. Fiorentino, J. Paxson, Optimization of the wound scratch assay to detect changes in murine mesenchymal stromal cell migration after damage by soluble cigarette smoke extract, *JoVE* 106 (2015), e53414.
- [16] Y. Sowa, T. Kishida, K. Tomita, K. Yamamoto, T. Numajiri, O. Mazda, Direct conversion of human fibroblasts into schwann cells that facilitate regeneration of injured peripheral nerve in vivo, *Stem Cells Transl Med* 6 (4) (2017) 1207–1216.
- [17] E.Z. Longa, P.R. Weinstein, S. Carlson, R. Cummins, Reversible middle cerebral artery occlusion without craniectomy in rats, *Stroke* 20 (1) (1989) 84–91.
- [18] T.W. Hsu, Y.J. Lu, Y.J. Lin, Y.T. Huang, L.H. Hsieh, B.H. Wu, Y.C. Lin, L.C. Chen, H.W. Wang, J.C. Chuang, Y.Q. Fang, C.C. Huang, Transplantation of 3D MSC/HUVEC spheroids with neuroprotective and proangiogenic potentials ameliorates ischemic stroke brain injury, *Biomaterials* 272 (2021), 120765.
- [19] Z. Jin, P. Guo, X. Li, J. Ke, Y. Wang, H. Wu, Neuroprotective effects of irisin against cerebral ischemia/reperfusion injury via Notch signaling pathway, *Biomed. Pharmacother.* 120 (2019), 109452.
- [20] M. Bieber, J. Gronewold, A.C. Scharf, M.K. Schuhmann, F. Langhauser, S. Hopp, S. Mencl, E. Geuss, J. Leinweber, J. Guthmann, T.R. Doeppner, C. Kleinschnitz, G. Stoll, P. Kraft, D.M. Hermann, Validity and reliability of neurological scores in mice exposed to middle cerebral artery occlusion, *Stroke* 50 (10) (2019) 2875–2882.
- [21] L. Wang, Y.L. Cho, Y. Tang, J. Wang, J.E. Park, Y. Wu, C. Wang, Y. Tong, R. Chawla, J. Zhang, Y. Shi, S. Deng, G. Lu, Y. Wu, H.W. Tan, P. Pawijit, G.G. Lim, H.Y. Chan, J. Zhang, L. Fang, H. Yu, Y.C. Liou, M. Karthik, B.H. Bay, K.L. Lim, S.K. Sze, C.T. Yap, H.M. Shen, PTEN-L is a novel protein phosphatase for ubiquitin dephosphorylation to inhibit PINK1-Parkin-mediated mitophagy, *Cell Res.* 28 (8) (2018) 787–802.
- [22] F.Y. Sun, X. Guo, Molecular and cellular mechanisms of neuroprotection by vascular endothelial growth factor, *J. Neurosci. Res.* 79 (1–2) (2005) 180–184.
- [23] G. van Weelden, M. Bobinski, K. Okla, W.J. van Weelden, A. Romano, J.M.A. Pijnenborg, Fucoidan structure and activity in relation to anti-cancer mechanisms, *Mar. Drugs* 17 (1) (2019).
- [24] Y. Xu, Y. Li, Q. Chen, L. Fu, L. Tao, Y. Wei, Injectable and self-healing chitosan hydrogel based on imine bonds: design and therapeutic applications, *Int. J. Mol. Sci.* 19 (8) (2018).
- [25] C. Frantz, K.M. Stewart, V.M. Weaver, The extracellular matrix at a glance, *J. Cell Sci.* 123 (Pt 24) (2010) 4195–4200.
- [26] T.Y. Wang, J.S. Forsythe, C.L. Parish, D.R. Nisbet, Biofunctionalisation of polymeric scaffolds for neural tissue engineering, *J. Biomater. Appl.* 27 (4) (2012) 369–390.
- [27] T.Y. Wang, J.S. Forsythe, D.R. Nisbet, C.L. Parish, Promoting engraftment of transplanted neural stem cells/progenitors using biofunctionalised electrospun scaffolds, *Biomaterials* 33 (36) (2012) 9188–9197.
- [28] I. Zvibel, F. Smets, H. Soriano, Anoikis, Roadblock to cell transplantation? *Cell Transplant.* 11 (7) (2002) 621–630.
- [29] T.E. Robey, M.K. Saiget, H. Reinecke, C.E. Murry, Systems approaches to preventing transplanted cell death in cardiac repair, *J. Mol. Cell. Cardiol.* 45 (4) (2008) 567–581.
- [30] M.H. Amer, F. Rose, K.M. Shakesheff, M. Modo, L.J. White, Translational considerations in injectable cell-based therapeutics for neurological applications: concepts, progress and challenges, *NPJ Regen Med* 2 (2017) 23.
- [31] L.M. Marquardt, V.M. Doulames, A.T. Wang, K. Dubbin, R.A. Suhar, M.J. Kratochvil, Z.A. Medress, G.W. Plant, S.C. Heilshorn, Designer, injectable gels to prevent transplanted Schwann cell loss during spinal cord injury therapy, *Sci. Adv.* 6 (14) (2020) eaaz1039.
- [32] Q. Feng, K. Wei, S. Lin, Z. Xu, Y. Sun, P. Shi, G. Li, L. Bian, Corrigendum to "Mechanically resilient, injectable, and bioadhesive supramolecular gelatin hydrogels crosslinked by weak host-guest interactions assist cell infiltration and in situ tissue regeneration" [*Biomaterials* 101C (2016) 217–228], *Biomaterials* 112 (2017) 346–347.
- [33] H. Wang, S.C. Heilshorn, Adaptable hydrogel networks with reversible linkages for tissue engineering, *Adv. Mater.* 27 (25) (2015) 3717–3736.
- [34] P.J. Psaltis, K.M. Peterson, R. Xu, F. Franchi, T. Witt, I.Y. Chen, A. Lerman, R.D. Simari, S.S. Gambhir, M. Rodriguez-Porcel, Noninvasive monitoring of oxidative stress in transplanted mesenchymal stromal cells, *JACC Cardiovasc Imaging* 6 (7) (2013) 795–802.
- [35] C.Y. Cho, T.H. Chiang, L.H. Hsieh, W.Y. Yang, H.H. Hsu, C.K. Yeh, C.C. Huang, J.H. Huang, Development of a novel hanging drop Platform for engineering controllable 3D microenvironments, *Front. Cell Dev. Biol.* 8 (2020) 327.
- [36] M. Kim, H.W. Yun, D.Y. Park, B.H. Choi, B.H. Min, Three-dimensional spheroid culture increases exosome secretion from mesenchymal stem cells, *Tissue Eng Regen Med* 15 (4) (2018) 427–436.
- [37] L. Xie, M. Mao, L. Zhou, B. Jiang, Spheroid mesenchymal stem cells and mesenchymal stem cell-derived microvesicles: two potential therapeutic strategies, *Stem Cell. Dev.* 25 (3) (2016) 203–213.
- [38] J. Herz, C. Koster, B.S. Reinboth, M. Dzietko, W. Hansen, H. Sabir, C. van Velthoven, I. Bendix, U. Felderhoff-Muser, Interaction between hypothermia and delayed mesenchymal stem cell therapy in neonatal hypoxic-ischemic brain injury, *Brain Behav. Immun.* 70 (2018) 118–130.
- [39] L. Bai, H. Shao, H. Wang, Z. Zhang, C. Su, L. Dong, B. Yu, X. Chen, X. Li, X. Zhang,

- Effects of mesenchymal stem cell-derived exosomes on experimental autoimmune uveitis, *Sci. Rep.* 7 (1) (2017) 4323.
- [40] F.H. Shamili, H.R. Bayegi, Z. Salmasi, K. Sadri, M. Mahmoudi, M. Kalantari, M. Ramezani, K. Abnous, Exosomes derived from TRAIL-engineered mesenchymal stem cells with effective anti-tumor activity in a mouse melanoma model, *Int. J. Pharm.* 549 (1–2) (2018) 218–229.
- [41] Z. Liu, M. Chopp, Astrocytes, Therapeutic targets for neuroprotection and neurorestoration in ischemic stroke, *Prog. Neurobiol.* 144 (2016) 103–120.
- [42] H.S. Kuehn, J.E. Niemela, K. Sreedhara, J.L. Stoddard, J. Grossman, C.A. Wysocki, M.T. de la Morena, M. Garofalo, J. Inlora, M.P. Snyder, D.B. Lewis, C.A. Stratakis, T.A. Fleisher, S.D. Rosenzweig, Novel nonsense gain-of-function NFKB2 mutations associated with a combined immunodeficiency phenotype, *Blood* 130 (13) (2017) 1553–1564.
- [43] J.D. Anderson, H.J. Johansson, C.S. Graham, M. Vesterlund, M.T. Pham, C.S. Bramlett, E.N. Montgomery, M.S. Mellema, R.L. Bardini, Z. Contreras, M. Hoon, G. Bauer, K.D. Fink, B. Fury, K.J. Hendrix, F. Chedin, S. El-Andaloussi, B. Hwang, M.S. Mulligan, J. Lehtio, J.A. Nolte, Comprehensive proteomic analysis of mesenchymal stem cell exosomes reveals modulation of angiogenesis via nuclear factor- κ B signaling, *Stem Cell.* 34 (3) (2016) 601–613.
- [44] G. de Couto, R. Gallet, L. Cambier, E. Jaghatspanyan, N. Makkar, J.F. Dawkins, B.P. Berman, E. Marban, Exosomal MicroRNA transfer into macrophages mediates cellular postconditioning, *Circulation* 136 (2) (2017) 200–214.
- [45] Y.S. Lee, A. Dutta, MicroRNAs in cancer, *Annu. Rev. Pathol.* 4 (2009) 199–227.
- [46] T. Barwari, A. Joshi, M. Mayr, MicroRNAs in cardiovascular disease, *J. Am. Coll. Cardiol.* 68 (23) (2016) 2577–2584.
- [47] C. Yapjajakis, Regulatory role of MicroRNAs in brain development and function, *Adv. Exp. Med. Biol.* 1195 (2020) 237–247.